ChemEngineering

MDPI

Article

Optimizing Chloride and Calcium Ion Extraction from Municipal Solid Waste Incineration Fly Ash from Zhoushan, China: Effects of Leaching Conditions and Industrial Applications

Kaicheng Zhang [1,†], Yecheng Xue [2,†], Dongyan Liu [2,*], Jianfu Zhao [3,*], Marta Sibhat [3] and Yang Tong [2]

[1] Department of Geography, Geomatics and Environment, University of Toronto Mississauga, Mississauga, ON L5L 1C6, Canada; cris.zhang@mail.utoronto.ca
[2] School of Environmental and Geographic Sciences, Shanghai Normal University, Shanghai 200092, China; 1000527438@smail.shnu.edu.cn (Y.X.); 1000549364@smail.shnu.edu.cn (Y.T.)
[3] College of Environmental Science and Engineering, Tongji University, Shanghai 200092, China; 2190016@tongji.edu.cn
* Correspondence: liudy@shnu.edu.cn (D.L.); zhaojianfu@tongji.edu.cn (J.Z.); Tel.: +86-18018673537 (D.L.)
† Co-first Authors: These authors contributed equally to this work.

Abstract: Municipal solid waste incineration (MSWI) fly ash, containing substantial amounts of calcium (Ca), chloride (Cl), and other valuable elements, offers promising potential as a raw material for carbon capture, utilization (CCU), and alkali production. Despite numerous approaches being explored to enhance calcium ion leaching from fly ash, the combined effects of salt and leaching conditions on ion extraction have not been thoroughly investigated. This study provides a comprehensive examination of various leaching conditions, including primary leaching—optimal for efficiency—secondary leaching, which achieved the highest leaching rate, and reverse secondary leaching, focusing on their impact on calcium extraction efficiency. Considering optimal leaching efficiency and resource utilization, this study identifies the most favorable industrial conditions as a 15 min leaching time, a stirring speed of 200 rpm, a temperature of 25 °C, and a 1:10 liquid-to-solid ratio (L/S ratio). The application of a 6% NaCl solution in salt-assisted leaching elevated the calcium ion concentration from 4101.5 mg/L to 4662.6 mg/L, indicating a substantial improvement in leaching performance. Additionally, in carbonate-assisted and ultrasound-assisted leaching, the introduction of CO_2 further increased calcium extraction amounts, but it did not enhance efficiency, while ultrasonic intervention had minimal impact. This research investigates enhanced efficiencies through multiple optimized and assisted leaching conditions, advancing MSWI fly ash utilization in carbon capture applications while paving new pathways for sustainable industrial practices that could revolutionize waste management and support global environmental objectives.

Keywords: ion extraction; leaching; MSWI fly ash; salt effect

Academic Editor: George Z. Papageorgiou

Received: 5 November 2024
Revised: 2 December 2024
Accepted: 19 December 2024
Published: 6 January 2025

Citation: Zhang, K.; Xue, Y.; Liu, D.; Zhao, J.; Sibhat, M.; Tong, Y. Optimizing Chloride and Calcium Ion Extraction from Municipal Solid Waste Incineration Fly Ash from Zhoushan, China: Effects of Leaching Conditions and Industrial Applications. *ChemEngineering* **2025**, *9*, 6. https://doi.org/10.3390/chemengineering9010006

1. Introduction

Municipal solid waste incineration (MSWI) fly ash is a byproduct originating mainly from the flue gases produced during the combustion of municipal waste [1]. During gas purification, solid particulate matter is captured by filters or electrostatic precipitators, resulting in the formation of MSWI fly ash [2]. Research by Yadav, et al. [3] and Gadore and Ahmaruzzaman [4] indicates that MSWI fly ash exhibits strong alkalinity. The associated hazards primarily arise from heavy metals like lead, cadmium, zinc, and copper, as well as organic pollutants, such as dioxins and furans. These substances can leach into the

environment, contaminating soil and water resources while posing significant health risks to humans and wildlife. Factors like pH and environmental chemicals influence the leaching of toxic substances, potentially increasing their mobility and amplifying environmental harm on a larger scale

Bottom ash frequently coexists with fly ash, both originating from MSWI waste incinerators. Recent studies demonstrate that treated and recycled MSWI bottom ash (MSWIBA) can be utilized to produce high-performance, compressed, stabilized earth blocks (CSEB) that exhibit superior strength in acid corrosion and moisture tests [5]. The strength of these CSEBs can be further augmented by incorporating specific amounts of cement to satisfy additional material requirements [6]. According to Tkachenko, et al. [7], global cement production is projected to reach 8.2 billion tons by 2030. Sufficient raw materials will be essential to support this substantial volume; however, their extraction can lead to significant environmental pollution and diminish economic benefits. After treatment, MSWI fly ash can serve as a raw material in cement and concrete production [8], as it contains numerous substances suitable for the industrial manufacturing of building materials like cement [9–11]. The use of treated MSWI fly ash significantly curtails mineral extraction in industrial manufacturing, offering considerable economic and environmental benefits by reducing raw material demands and minimizing waste disposal [12,13]. Given that fly ash is suitable for cement production, integrating fly ash and bottom ash into a single site for manufacturing could streamline the production process and eliminate transportation costs associated with industrial production.

Despite its advantages, MSWI fly ash often contains significant impurities, including calcium and chloride salts, such as $CaSO_4$, CaCl(OH), $CaCO_3$, SiO_2, NaCl, and KCl [13,14]. These salts can compromise the quality of fly ash as a concrete raw material during industrial use and must be removed through water leaching [15] to enhance the speed and quality of subsequent production [16]. Ongoing efforts aim to reduce costs and enhance environmental benefits in the current production process [17,18].

Traditional treatment methods for MSWI fly ash currently focus on stabilizing and reducing the leachability of its hazardous constituents. A prevalent approach is thermal treatment, which involves heating the ash to high temperatures to immobilize heavy metals and eliminate organic contaminants [19]. Xu, Wang, Zeng, Zhao, Wang, Zhan, Li and Yang [18] demonstrated that microwave-assisted heat treatment effectively controls heavy metal contamination in fly ash, significantly enhancing the stability of metals like mercury, lead, cadmium, and zinc. Another widely employed method is hydrometallurgy, which uses acids like nitric acid to leach heavy metals from ash, achieving high removal efficiencies for metals like lead, cadmium, copper, and zinc [20,21]. In addition, biometallurgy offers greater environmental benefits despite a lower recovery rate of only 46%. Utilizing Aspergillus niger and a sucrose solution results in organic waste throughout all steps, further enhancing process sustainability. However, these methods primarily target directly harmful substances like heavy metals and dioxins while neglecting the removal efficiency of ions, such as calcium ions and chloride ions.

Leaching is a vital pre-treatment process for eliminating soluble salts and heavy metals from MSWI fly ash. This process involves washing the fly ash with water or other solvents to dissolve and eliminate impurities. Leaching enhances both the environmental safety of fly ash and the quality and properties of the final construction material [22]. Ions present in fly ash, such as chloride and calcium ions, can influence cement properties when used as a raw material. Chloride ions can induce corrosion in steel reinforcement, significantly reducing reinforced concrete strength and posing safety risks. In contrast, calcium ions can create air bubbles within the cement matrix, leading to a significant decline in cement strength. Other heavy metals can leach into the environment, causing significant environmental and

health issues [16,23]. Therefore, leaching is crucial as a precursor to industrial applications of fly ash, ensuring its safe use in construction materials. After leaching, residual fly ash can be repurposed as an industrial material. The alkaline leachate, containing $Ca(OH)_2$ and high concentrations of NaCl with elevated material concentration and conductivity, can serve as a solvent for industrial carbon capture and alkali production [24].

This study explores salt-assisted leaching, specifically utilizing NaCl, to enhance calcium extraction. Current research primarily focuses on leaching heavy metals from MSWI fly ash through chemical and thermal treatments. Studies have documented that both NaCl and Na_2SO_4 enhance heavy metal leaching, suggesting that Cl^- ions may improve leaching efficiency [25,26]. However, most studies have not explored optimal conditions, like the NaCl solution's concentration, to maximize the salt effect's effectiveness, nor have they thoroughly explained the detailed ion extraction mechanism. Instead, studies often emphasize broader approaches like electrodialysis treatment, which can effectively remove significant heavy metals from fly ash [26]. This highlights a gap in the literature and underscores the need for further research on effectively using NaCl to enhance ion extraction efficiency from MSWI fly ash. This study aims to address this gap by systematically investigating primary, secondary, and reverse secondary leaching to determine optimal conditions, such as the leaching time, stirring speed, temperature, and liquid-to-solid ratio. The introduction of additional Cl^- ions was also explored to maximize calcium extraction efficiency. Additionally, carbonate-assisted and ultrasound-assisted leaching were explored to identify further performance enhancements. This research demonstrates that significant improvements in leaching efficiency through the salt effect can be combined with other methods targeting heavy metals and other elements. This forms a comprehensive process for industrialized fly ash treatment, simplifying the treatment process while yielding significant economic and environmental benefits.

2. Materials and Methods

2.1. Materials

The fly ash used in this experiment was obtained from the Zhoushan Waste Incineration Plant in China and had been stored for two months (Figure 1). The fly ash was characterized by its fine particle size, black-gray color, and a moisture content of 0.17% after being heated to a constant temperature of 105 °C in a drying oven.

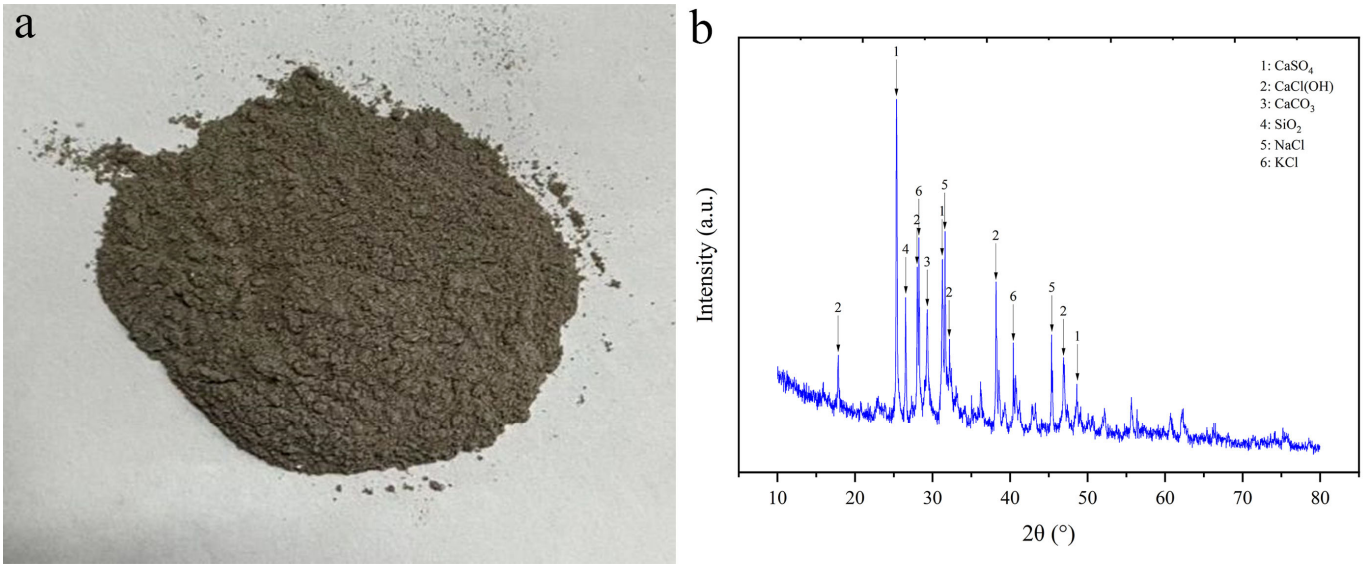

Figure 1. Original fly ash (**a**) brownish-black dry powder; (**b**) XRD plot.

Table 1 presents the metal composition and content of the fly ash, which align with the findings of Cho, Nam, An and Youn [9]. Powder X-ray diffraction (XRD) analysis of the air-dried salt residue post-leaching revealed that the predominant salt components in the fly ash leach solution were $CaSO_4$, NaCl, KCl, and CaCl(OH). These chloride and calcium ions are essential for enhancing leaching efficiency.

Table 1. Components of the fly ash based on XRF.

Element	O	Ca	Na	Mg	Si	S	Cl	K	Fe	Cu	Zn	Pb
Weight percentage (%)	37.07	29.9	3.39	0.91	2.68	7.7	11.52	2.03	2.09	0.07	0.38	0.14

2.2. Experiment Method

The primary leaching experiments adhered to a standard protocol. Before leaching, all fly ash samples were dried in an oven at 105 °C for 24 h to achieve a constant weight. Each dried sample was weighed and placed into a beaker, mixed with distilled water at specific liquid–solid (L/S) ratios, and then thoroughly agitated using a mechanical stirrer. For experiments requiring temperature control, the beaker and the distilled water were pre-heated to the target temperature before the fly ash was added. The primary leaching variables included temperatures of 10, 30, 50, 70, and 90 °C; L/S ratios from 1:2 to 1:50; stirring speeds from 0 to 400 rpm; and leaching times from 5 to 150 min. Upon completion of leaching, the leachate was filtered from the solid residue using a vacuum extractor.

In carbonate-assisted leaching experiments, samples were prepared similarly to the standard process but transferred to a three-port flask filled with distilled water. One port of the flask was connected to carbon dioxide and nitrogen gas cylinders via an aeration head, with an electronic gas flow meter monitoring CO_2 flow rates. The second port, connected to a mechanical stirrer, provided continuous stirring during leaching, while the third port, connected to a pH meter, monitored pH changes, as shown in Figure 2. In this setup, CO_2 and N_2 were mixed at a volume ratio of 14% to 86%. The leaching temperature was maintained at 25 °C, the stirring speed at 200 rpm, the L/S ratio at 1:10, and the leaching time at 15 min. CO_2 flow rates of 100, 200, and 300 mL/min were tested.

For ultrasound-assisted leaching research, fly ash samples were prepared following the standard leaching process and then placed in an ultrasound generator. This setup enabled leaching both with and without ultrasound assistance by applying an ultrasound frequency of 40 kHz. Experimental conditions included a leaching temperature of 25 °C, a stirring speed of 200 rpm, an L/S ratio of 1:10, and a leaching time of 15 min.

For secondary leaching, samples were prepared following the standard procedure but using fly ash residue that had been previously leached. In this experiment, only the L/S ratio was varied—1:2, 1:4, 1:6, 1:8, 1:10, 1:15, and 1:20—matching the solid–liquid ratios used in primary leached fly ash. The temperature was maintained at 25 °C, the stirring speed at 200 rpm, and the leaching time at 15 min for both primary and secondary leaching.

For reverse secondary leaching (RSL), samples followed the standard procedure but used secondary leachate as the solvent. In this experiment, only the L/S ratio varied from 1:2 to 1:20, matching those used in primary leached fly ash. The temperature was maintained at 25 °C, the stirring speed at 200 rpm, and the leaching time at 15 min for both primary and secondary leaching.

In salt effect experiments, distilled water was replaced with NaCl solutions at concentrations of 2%, 4%, 6%, 8%, 10%, 15%, and 20% to evaluate salt's influence on leaching efficiency.

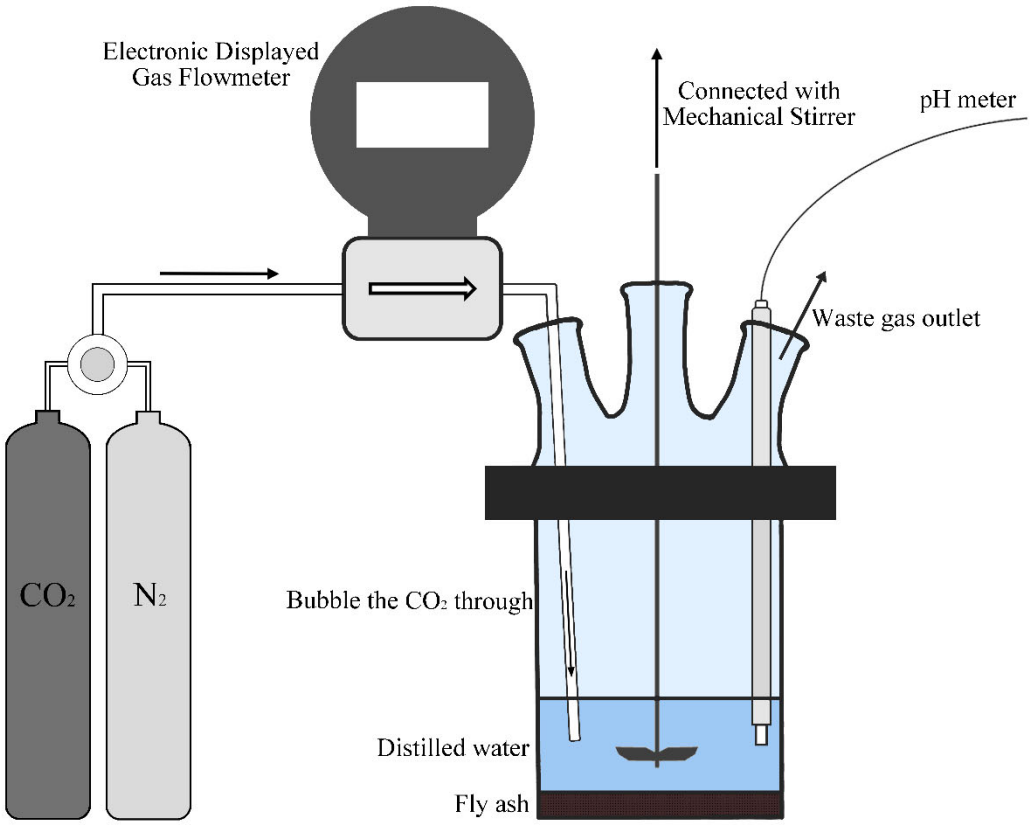

Figure 2. Experimental setup for carbonate-assisted leaching.

To determine the total chloride ion concentration, a 0.5 mol/L sulfuric acid solution was added to a beaker containing the fly ash sample. The leaching process occurred at a constant temperature of 25 °C with a stirring speed of 200 rpm and a duration of 15 min.

2.3. Data Analysis

To evaluate leaching efficiency under different conditions, the relative leaching rate (φ) was calculated as the ratio of the total mass of chloride ions leached from fly ash to that of a reference sample. This value, expressed as a percentage, was calculated using the following formula:

$$\varphi = \frac{m_{leach}}{m_{total}} \times 100\% \quad (1)$$

Here, m_{leach} represents the mass of leached chloride ions (mg) in each experimental group, and m_{total} denotes the mass concentration of leached chloride ions (mg) in the test group.

In these experiments, most chloride ions in fly ash existed as soluble chloride salts, which were effectively removed through leaching. In contrast, most calcium ions were present as calcium carbonate, which is insoluble in water and thus not easily removed through leaching. Consequently, chloride ion leaching efficiency was expressed as a percentage, whereas calcium ion concentrations were measured in mg/L.

2.4. Analytical Methods

i. Standard Ion Test Methods

To determine the concentration of chloride ions (Cl^-), a 50 mL solution was prepared and diluted with distilled water if necessary to reduce the chloride content. Subsequently, 1 mL of a 5% potassium chromate (K_2CrO_4) solution was added. Titration was conducted using a 0.0141 M standard silver nitrate ($AgNO_3$) solution until a brick-red precipitate

formed, indicating the endpoint. This method conformed to the Chinese National Standard GB 11896-89 [27].

For assessing calcium ions (Ca^{2+}), a 50 mL solution was prepared. After adding 1 mL of a 1 M sulfuric acid (H_2SO_4) solution and 5 mL of a 4% potassium persulfate ($K_2S_2O_8$) solution, the mixture was heated until nearly dry. Once cooled to room temperature, 50 mL of distilled water, 3 mL of triethanolamine solution, 7 mL of a 0.1 M potassium hydroxide (KOH) solution, and 0.2 g of calcium hydroxide ($Ca(OH)_2$) indicator were added. The solution was titrated with a 0.01 M EDTA standard solution until a color change from purple to bright blue indicated the endpoint. This method conformed to the Chinese National Standard GB/T 15452-2009 [28].

For hydroxide ion (OH^-) determination, a 50 mL sample was prepared with 3–4 drops of a 1% phenolphthalein solution added. Once the solution turned red, it was titrated with a 0.05 M standard hydrochloric acid (HCl) solution until the red color disappeared. Then, four drops of a 0.05% methyl orange solution were added, and titration continued with hydrochloric acid until a distinct color change from yellow to orange indicated the endpoint. This method conformed to the Chinese Geological and Mineral Industry Standard DZ/T 0064.49-93 [29].

ii. Characterization

Laser particle size analysis of both original and washed fly ash was performed using the Malvern Mastersizer 2000 and Scirocco 2000 systems. The detection range was 0.02 to 2000 µm, with an obscuration rate of 1.05%, a weighted residual of 0.816%, zero absorption, and a particle refractive index (RI) of 1.5.

X-ray diffraction (XRD) analysis of both original and washed fly ash was performed using a Rigaku SmartLab SE with Cu-Kα radiation as the X-ray source. The scanning range was from $2\theta = 10^\circ$ to 80° at a speed of 2°/min, with a tube current of 50 mA and the voltage set at 40 kV.

The chemical composition of fly ash samples was determined using an X-ray fluorescence (XRF, ZSX Primus III+) system via the pressed pellet method. This method utilized a lens diameter of 20 mm and covered a scanning range from oxygen (O) to uranium (U).

Scanning electron microscopy (SEM) was performed using a ZEISS Sigma 300 to characterize the surface topography of fly ash samples by employing field emission techniques.

3. Results and Discussion

3.1. Primary Leaching

i. Effect of leaching time

Titration data show that leaching efficiencies for both chloride and calcium ions increased with leaching times up to 60 min, achieving maximum values of 87.75% for chloride ions and 4141.6 mg/L for calcium ions. These results align with other reported leaching efficiencies in the literature. However, after 60 min, a slight decrease in the leaching of both chloride and calcium ions was observed. The leaching percentage of chloride ions decreased by 1.01%, while the calcium ion concentration decreased by 87.5 mg/L between 60 and 150 min, as shown in Figure 3.

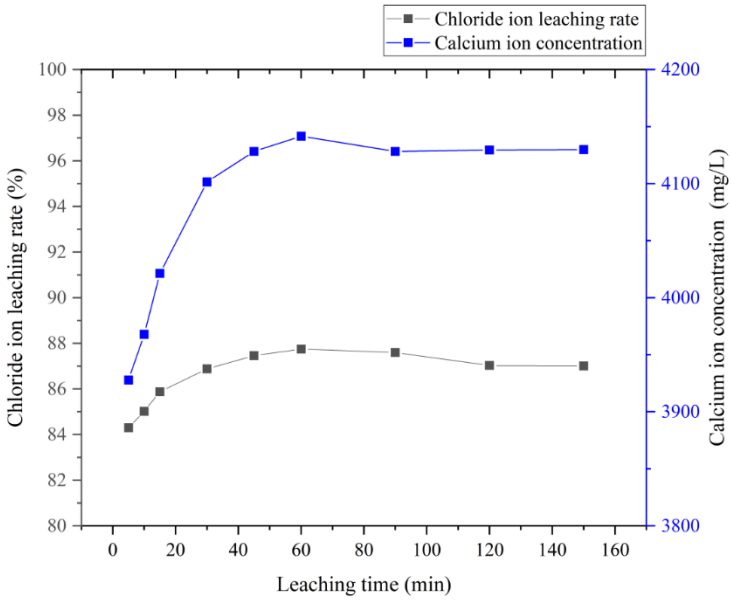

Figure 3. Effect of leaching time on leaching efficiency of chloride and calcium ions.

To optimize energy consumption related to stirring, a standard duration of 15 min was chosen. The difference in leaching efficiency between the standard 15 min duration and the maximum chloride ion leaching at 60 min was 1.83%, while for calcium ions it was 162.5 mg/L. These differences are negligible compared to the total leaching amounts under certain conditions. This approach ensures economic efficiency and minimizes the impact of extraneous factors on experimental outcomes.

Some chloride ions formed insoluble salts within the leach solution, reducing the detectable chloride ion concentration. Calcium ions (Ca^{2+}) react with CO_2 in the air after 60 min, forming $CaCO_3$ precipitate and decreasing the concentration. CaCl(OH) converted to $Ca(OH)_2$ and $CaCl_2$ during prolonged leaching, reaching equilibrium after 60 min, as described by Jiménez, et al. [30,31]:

$$2\,CaCl(OH)_{(aq)} \leftrightarrow Ca(OH)_{2(s)} + CaCl_{2(aq)} \quad (2)$$

At this stage, the solution contains CaCl(OH), $Ca(OH)_2$, $CaCl_2$, and $CaSO_4$. $Ca(OH)_2$ reacts with CO_2 in the air to form a $CaCO_3$ precipitate, reducing the concentration. In industrial applications, a leaching time of no more than 60 min should be selected to achieve optimal leaching rates. At this point, both Cl^- and Ca^{2+} ions reach peak leaching rates simultaneously. The subsequent reaction with CO_2 to form $CaCO_3$ can be managed through later processes, like carbon capture from leachate, eliminating the need for extended leaching time for less efficient $CaCO_3$ precipitation [32].

ii. Effect of stirring speed

Existing research has provided ample discussion and clear conclusions regarding the effects of the leaching temperature, the L/S ratio, and the leaching time on the leaching efficiency of Cl^- and Ca^{2+} ions. However, the impact of the stirring speed has not been thoroughly examined. Huang, et al. [33] reported that a leaching efficiency of 88.72% can be achieved with an L/S ratio of 8:1, a leaching time of 5 min, and a leaching temperature of 70 °C. This leaching rate aligns with our experimental results; however, their stirring speed was 1200 rpm. High stirring speeds may cause liquid splashing, affecting leaching efficiency and introducing errors.

Too low a stirring speed can lead to inadequate agitation of fly ash, causing partial precipitation in the leaching solution and significantly reducing the leaching efficiency. Con-

sequently, the leaching efficiency for chloride and calcium ions increases rapidly between 0 and 100 rpm. The rate of increase slows beyond 100 rpm, reaching an inflection point at 150 rpm. Beyond 200 rpm, chloride ion leaching efficiency stabilizes at 90% ± 0.5%, while the calcium ion concentration remains constant at 4110 ± 10 mg/L. After 200 rpm, chloride ion leaching efficiency stabilizes further; increasing the speed offers minimal improvement in performance. For each additional 50 rpm increase, the chloride ion leaching rate increases by less than 0.3%, which is insufficient to justify additional energy consumption. Each additional increase beyond this results in less than a 0.3% gain in chloride ion leaching (Figure 4). Stirring speeds above 200 rpm lead to higher energy consumption; thus, a stirring speed of 200 rpm was selected as the most cost-effective standard condition for subsequent experiments.

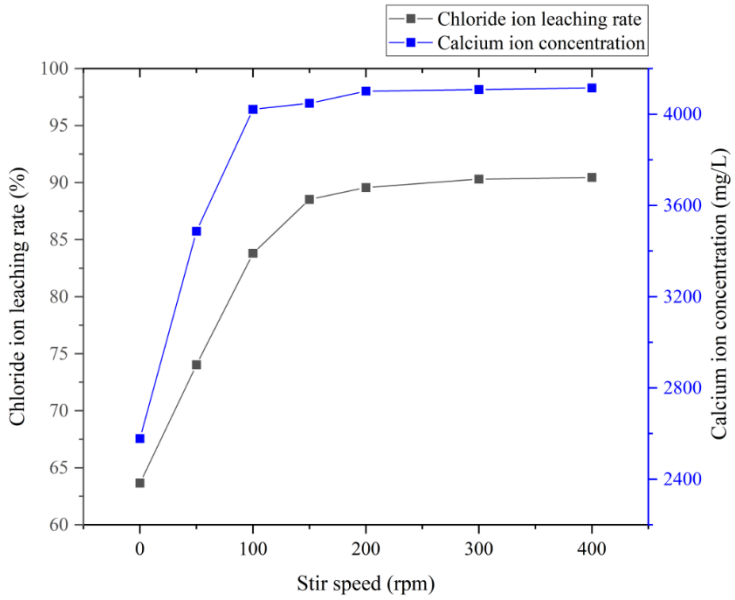

Figure 4. Effect of stirring speed on leaching efficiency of chloride and calcium ions.

iii. Effect of leaching temperature

The leaching temperature had opposing effects on the efficiencies of chloride and calcium ion leaching, with chloride ion efficiency reaching a peak of approximately 87.18% at 50 °C. Above 50 °C, the efficiency of chloride ion leaching slightly decreased due to the increased solubility of NaCl with rising temperatures (Figure 5). As the solubility of $Ca(OH)_2$ and $CaSO_4$ decreases with increasing temperature, most calcium ions precipitate at higher temperatures, reducing free calcium ion concentrations in the solution and causing a rapid decline in their leaching efficiency. Raising the temperature from 10 °C to 30 °C resulted in a 3.02% increase in the chloride ion leaching rate and a reduction of 53.4 mg/L in the calcium ion concentration. Further elevating the temperature from 30 °C to 50 °C resulted in just a 0.29% increase in the chloride ion leaching rate, while the calcium ion concentration fell by 66.8 mg/L. These findings indicate that beyond 30 °C, additional temperature increases offer minimal improvement in chloride ion leaching efficiency but lead to a more significant decrease in calcium ion leaching efficiency. In an industrial setting, increasing the temperature demands significant energy; because chloride ion leaching efficiency gains are negligible above 30 °C and come at the expense of reduced calcium ion efficiency, further temperature elevation is not energy-efficient. Moreover, at 30 °C, both chloride and calcium ion leaching results are satisfactory. This temperature strikes an optimal balance between maximizing chloride ion leaching efficiency and minimizing energy consumption while maintaining an acceptable level of calcium ion leaching.

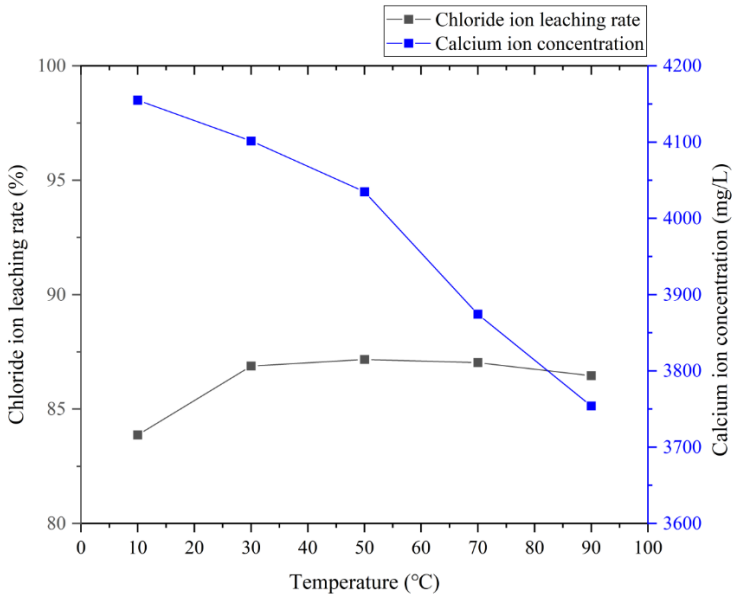

Figure 5. Effect of leaching temperature on leaching efficiency of chloride and calcium ions.

iv. Effect of liquid-solid ratio (L/S ratio)

The liquid-to-solid (L/S) ratio is positively correlated with the leaching efficiencies of both chloride and calcium ions. A lower L/S ratio leads to a greater retention of water and ions in the wet fly ash residue following vacuum filtration. Starting with 10 g of fly ash, 11.5 ± 0.5 g remained post-vacuum filtration, and 8.5 ± 0.3 g remained after drying, indicating that approximately 3 ± 0.8 g of water was retained in the residue. A higher proportion of ions retained in moisture within the fly ash residue decreases the ion concentration in the leaching solution, resulting in lower chloride ion leaching efficiencies at low L/S ratios compared to normal values, with initial rapid increases observed as L/S ratios rise. Calcium ions exhibited similar trends; however, their initial rapid increase in leaching efficiency was attributed to the saturation levels of $Ca(OH)_2$ and $CaCl_2$ in suspension [34,35]. Alterations in the L/S ratio did not affect the concentration of dissolved calcium ions; however, their total amount increased rapidly with rising L/S ratios, as illustrated in Figure 6. Thus, theoretically, a higher L/S ratio can achieve an increased leaching rate within a single leaching process. This indicates that while using substantial amounts of water in industrial processes can reduce the processing time and costs, environmental and economic concerns associated with high water consumption must be addressed.

v. Characteristics of residue

SEM images show that the sizes of individual fly ash particles vary widely, ranging from 10 to 200 μm in diameter. The surface texture features a mix of small, jagged, and smooth elements, with pits measuring 3 to 6 μm and protrusions ranging from 0.5 to 2 μm. These protrusions are needle-like and blocky, with smaller ones clustering into spherical masses adhering to the fly ash surface, reaching heights of about 1 to 3 μm. After a standard primary leaching process, fly ash particle sizes remain largely unchanged; however, most jagged edges and pits become filled, creating a smoother overall surface [33]. Needle-like protrusions shorten to less than 1 μm in length, while blocky protrusions shrink to between 0.1 and 1 μm (see Figure 7).

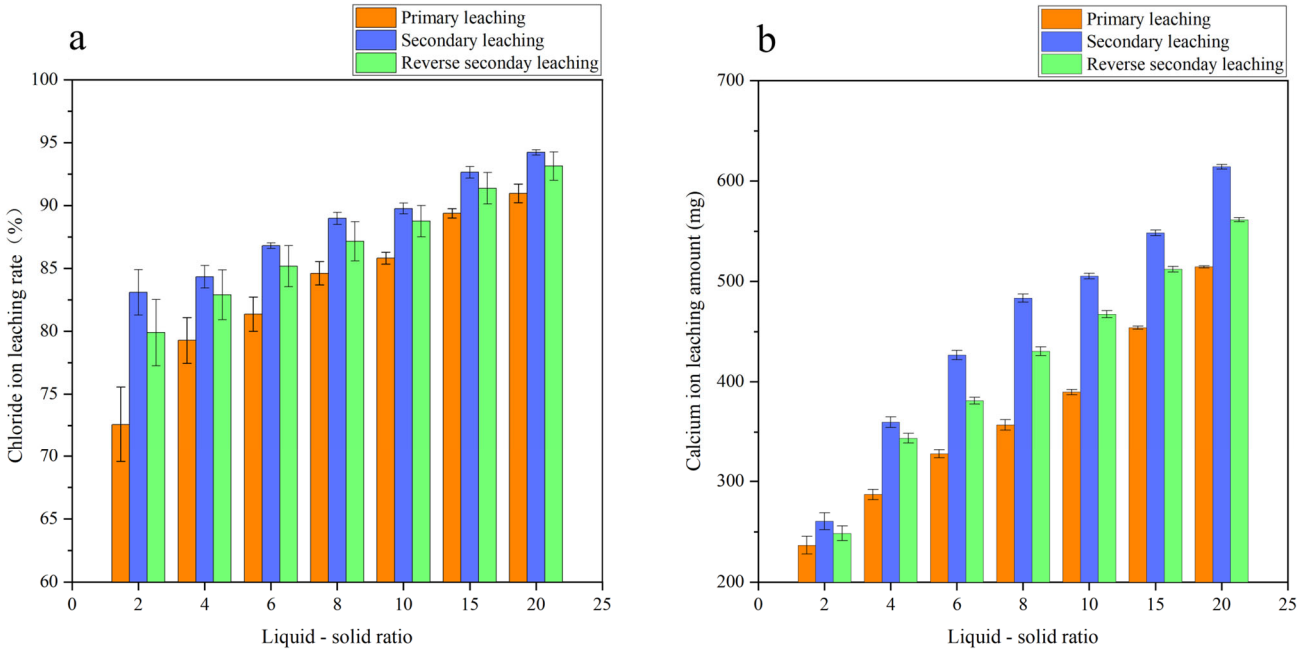

Figure 6. Effect of L/S ratio on leaching efficiency of (**a**) chloride ion; (**b**) calcium ions.

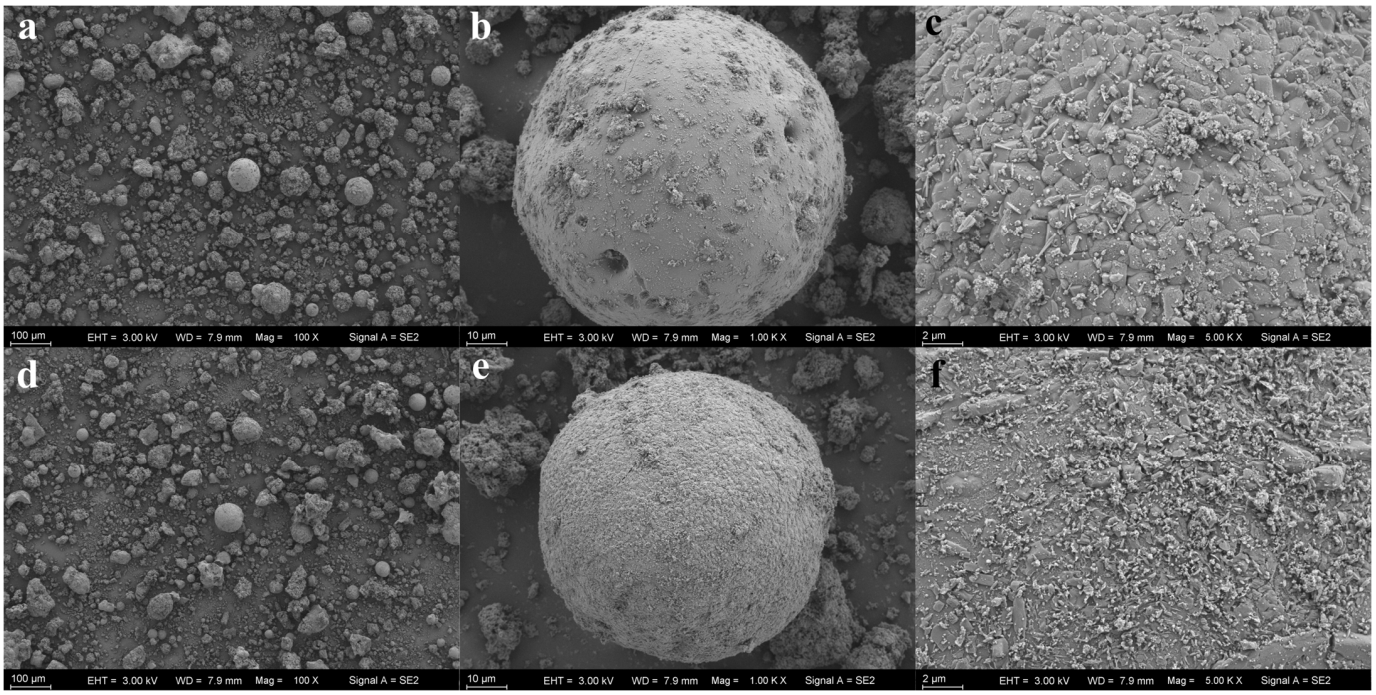

Figure 7. SEM images comparing fly ash before and after primary leaching. (**a**) Before leaching (100 μm). (**b**) Before leaching (10 μm). (**c**) Before leaching (2 μm). (**d**) After leaching (100 μm). (**e**) After leaching (10 μm). (**f**) After leaching (2 μm).

In original fly ash, both needle-like and massive surface protrusions comprise mixtures of soluble and insoluble salts. These were separated and dissolved through water washing and agitation, leading to an increased number of smaller protrusions.

3.2. Secondary Leaching and Reverse Secondary Leaching

The images demonstrate that secondary leaching achieves superior leaching efficiencies for both chloride and calcium ions compared to primary leaching. Attaining these high leaching efficiencies requires substantial quantities of pure water, which increases indus-

trial costs and exerts significant pressure on water resources, thus raising environmental concerns [36,37]. This study introduces reverse secondary leaching (RSL), which employs leachate from secondary leaching to process original fly ash, achieving leaching efficiencies between primary and secondary leaching.

Variations in chloride ion leaching efficiencies between reverse secondary and primary or secondary processes are primarily due to NaCl and CaCl(OH), whereas differences in calcium ion efficiencies are mainly attributed to $CaCl_2$ and $Ca(OH)_2$. In primary and secondary leaches, suspensions become saturated with $CaCl_2$ and $CaSO_4$, enabling the extraction of portions of saturated chloride and calcium ions at each stage. As a result, secondary leaching demonstrates greater efficiency than primary leaching [36]. Thus, RSL efficiency falls between that of primary and secondary leaching because it employs solvent from secondary processes to extract additional chloride and calcium ions. Ultimately, this results in an efficiency higher than that of primary but lower than that of secondary leaching (Figure 6).

Experimental results reveal a clear trend indicating that increasing the L/S ratio enhances the leaching efficiencies of both chloride and calcium ions. After primary leaching, secondary processes further extract additional chloride and calcium ions. This method bypasses primary processes by utilizing only secondary leaching, reversing with its own leachate to establish a production cycle (Figure 8). This production cycle achieves greater efficiency than primary methods while significantly reducing water usage and mitigating potential environmental impacts.

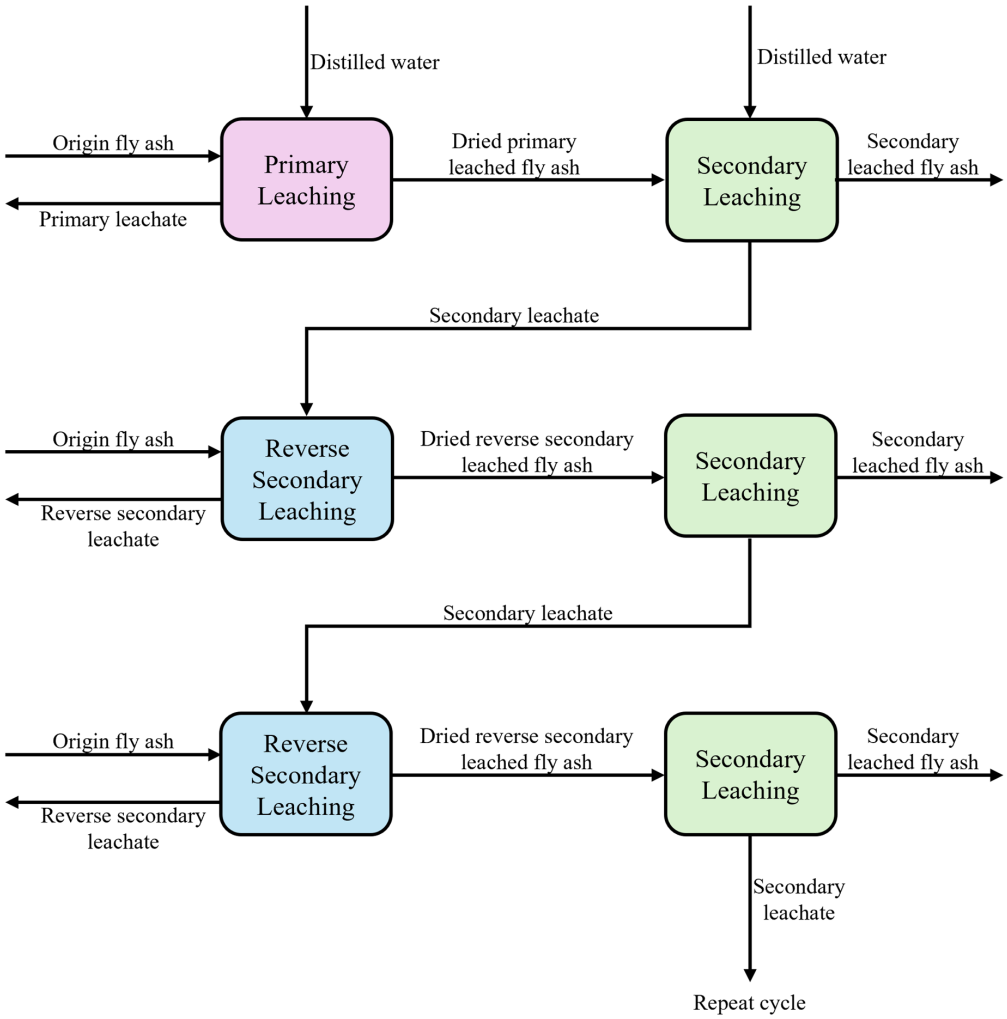

Figure 8. Secondary and inverse secondary industrial cycles.

The existing method utilizing Na_2CO_3 solution and deionized water was enhanced by incorporating reverse secondary leaching (RSL). Although the method employing Na_2CO_3 solution exhibits a limited calcium ion removal rate due to the formation of $CaCO_3$ precipitate, our approach achieves a high calcium ion leaching rate despite a relatively low chloride ion leaching rate [38]. Our study also emphasizes the importance of optimizing the stirring speed and the temperature to ensure economic efficiency without compromising leaching performance. A stirring speed of 200 rpm and a temperature of 30 °C were identified as optimal conditions, balancing maximum ion removal with minimal energy consumption. This study presents a comprehensive and economically viable method for effectively removing Ca^{2+} and Cl^- ions from fly ash, with potential applications in industrial settings where efficient extraction of these ions is essential.

While RSL can reduce water usage by reusing leachate, it still demands substantial amounts of pure water, potentially leading to increased industrial costs and exerting pressure on water resources, thus posing significant environmental challenges. Moreover, RSL's efficiency falls between that of primary and secondary leaching, potentially limiting its effectiveness in scenarios requiring maximum extraction efficiency. The complexity of the process may elevate operating costs and necessitate sophisticated management systems. Furthermore, dependence on saturation levels of compounds like $CaCl_2$ and $CaSO_4$ necessitates precise control, which can be challenging in large-scale applications.

3.3. Salt Effect Research

This experiment sought to examine the impact of introducing an additional chloride ion source on the leaching efficiency of calcium ions. Chloride ions from added NaCl were anticipated to exert a salting effect on $CaSO_4$ and CaCl(OH) in the leaching solution. Additionally, this increases the electrolyte concentration for subsequent electrolysis, potentially enhancing treatment efficiency. Because CaCl(OH) contains chloride ions, NaCl or any Cl-containing salt induces a salting effect that reduces its solubility, leading to precipitation and decreasing detectable hydroxide ion concentrations in solution [39]. Conversely, NaCl exerts a salt-solubilizing effect on CaSO4, enhancing its solubility and increasing sulfate ion concentrations in solution. At lower NaCl concentrations, hydroxide ion levels decrease gradually; however, as the NaCl concentration rises, they decline more rapidly. In contrast, as illustrated in Figure 9, sulfate ion levels rise quickly initially before stabilizing.

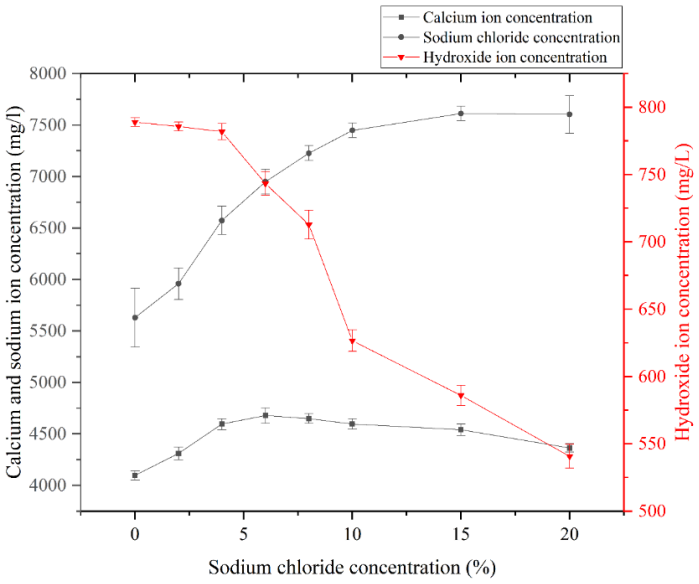

Figure 9. Effect of different concentrations of NaCl solution as leaching solvent on the leaching of hydroxide ions, sulfate ions, and calcium ions.

The salting effect of NaCl influences both $CaSO_4$ and $Ca(OH)_2$. With an increasing NaCl concentration, the leaching concentration of $CaSO_4$ increases, whereas that of $Ca(OH)_2$ decreases. These combined effects lead to an initial increase in calcium ion leaching concentrations, which peak at a 6% NaCl concentration, followed by a subsequent decrease [40]. In a 0% NaCl solution (pure H_2O), Ca^{2+} leaching was measured at 4101.52 mg/L; it peaked at 4662.64 mg/L with a 6% NaCl concentration, representing an increase of 561.12 mg/L or 13.68% above the baseline. Beyond a 6% NaCl concentration, leaching amounts gradually decreased, reaching 4368.72 mg/L at a 20% NaCl concentration. This change is significant when compared to the initial leaching values. XRD analysis indicates that higher NaCl concentrations are associated with increased $Ca(OH)_2$ peaks, supporting these findings (see Figure 10d,e). For fly ash, a higher rate of calcium ion removal offers greater benefits for industrial reuse. A high removal rate can reduce both the time and economic costs associated with processing fly ash, thereby enhancing its utilization efficiency. Therefore, a 6% NaCl solution, which represents the highest Ca^{2+} ion removal rate, was selected for industrial leaching based on its salting effect.

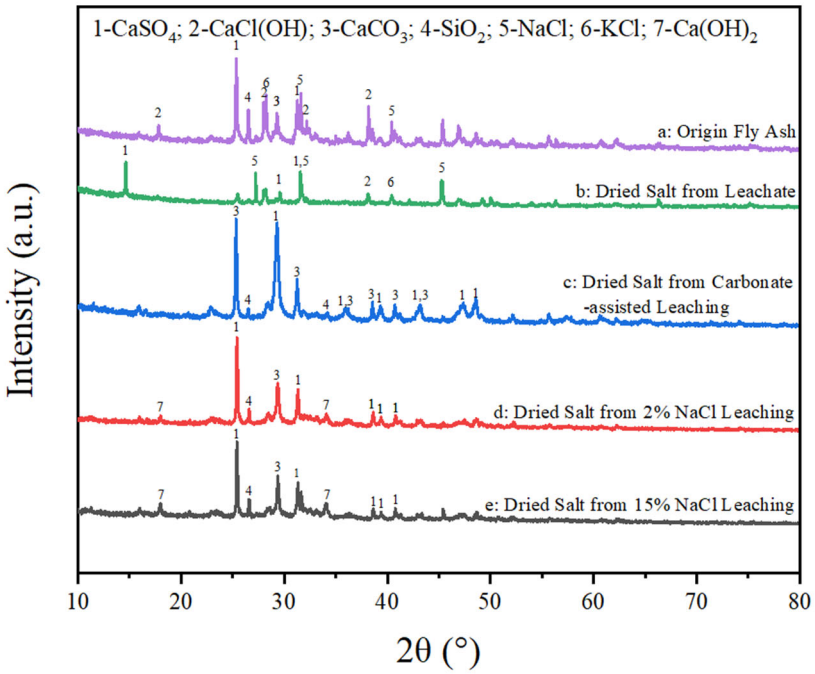

Figure 10. (a) XRD plots of (a) original fly ash; (b) dried salts from leachate; (c) carbonate-assisted leachate salts; (d) salts from low (2%) NaCl leach; (e) salts from high (15%) NaCl leach.

The study's findings underscore the substantial impact of the NaCl concentration on the efficiency of calcium ion leaching from compounds like $CaSO_4$ and $Ca(OH)_2$, which is crucial for industrial scalability and economic considerations. An optimal NaCl concentration of 6% yields the highest calcium ion removal rate, thereby enhancing the potential for industrial reuse of materials like fly ash. This concentration strikes a balance between maximizing leaching efficiency and managing costs, as further increases in the NaCl concentration lead to diminishing returns. However, economic trade-offs involve the cost of bulk NaCl, the precise process control needed to maintain optimal conditions, and potential environmental impacts from increased salinity in the waste stream. These issues may be mitigated by integrating this process with others that generate NaCl as a byproduct. Additionally, implementing this process on an industrial scale may necessitate infrastructure modifications to accommodate specific process requirements and subsequent treatments, like electrolysis.

3.4. Carbonate-Assisted Leaching

During the leaching process, carbon dioxide gas reacts with $Ca(OH)_2$ and CaCl(OH) in the leach solution, resulting in the formation of calcium carbonate, calcium chloride, and water [16,20,30,41]:

$$2\,CaCl(OH)_{(aq)} + 2\,H_2O_{(l)} \rightarrow Ca(OH)_{2(aq)} + CaCl_2{\cdot}2\,H_2O_{(aq)} \quad (3)$$

$$Ca(OH)_{2(aq)} + CO_{2(g)} \rightarrow CaCO_{3(s)} + H_2O_{(l)} \quad (4)$$

$$2\,CaCl(OH)_{(aq)} + CO_{2(g)} \rightarrow CaCO_{3(s)} + CaCl_{2(aq)} + H_2O_{(l)} \quad (5)$$

As shown in Figure 11, increasing the gas flow rate enhances the cavitation effects, thereby significantly improving the efficiency of chloride ion leaching. The reduction in hydroxide ions can be assessed through pH values, taking into account the rates of CO_2 introduction and utilization.

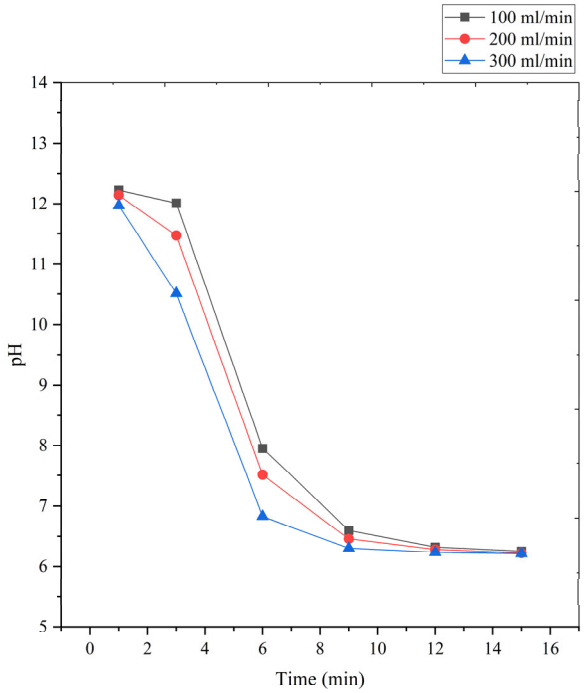

Figure 11. Effect of carbonate-assisted on leaching efficiency, illustrated by the changing of the pH value.

XRD analysis (see Figure 10c) revealed that after drying, the carbonated leach solution contains significant amounts of $CaCO_3$ and $CaSO_4$ but lacks $Ca(OH)_2$ [42]. The pH stabilizes after six minutes as hydroxide ions from $Ca(OH)_2$ are depleted, while dissolved CO_2 forms carbonic acid. Moreover, the influx of carbon dioxide also affects Ca^{2+} and Cl^- ions. Four sets of experimental data were collected for analysis; the following data represent averages from the first, second, and fourth datasets. The 100 mL/min segment of the third dataset displayed clear anomalies, with a Ca^{2+} ion concentration of 2902 mg/L, a Cl^- ion concentration of 7398 mg/L, and a Cl^- ion leaching rate of 87.66%. These values significantly differed from the averages of the other three groups and were thus considered experimental errors. Although no errors were apparent in the data from the 200 mL/min and 300 mL/min groups, uncertainty remained regarding concurrent errors in the 100 mL/min group; therefore, this dataset was excluded from calculations (see Table 2). Calcium ion leaching slightly decreased as calcium hydroxide absorbed carbon dioxide to form a precipitate. The influx of carbon dioxide induced cavitation effects that increased chloride ion leaching by 1.2%.

Table 2. The effect of the speed of carbon dioxide permeation on the leaching of Ca^{2+} and Cl^-.

CO_2 Passing Rate (mL/min)	Ca^{2+} Ion Concentration (mg/L)	Cl^- Ion Concentration (mg/L)	Cl^- Ion Leaching Rate
100	3341.67	8110.33	96.18%
200	3402.67	8226.33	97.38%
300	3347	8218	97.38%

SEM images reveal that carbonate-assisted leaching significantly increases the roughness of fly ash particles compared to standard primary leaching, resulting in jagged surfaces with cracks measuring 2–5 μm in length. Protrusions and surface jaggedness were transformed into needle-like formations, comparable in number to those observed in primary leaching, with lengths ranging from 0.3 to 1 μm (see Figure 12).

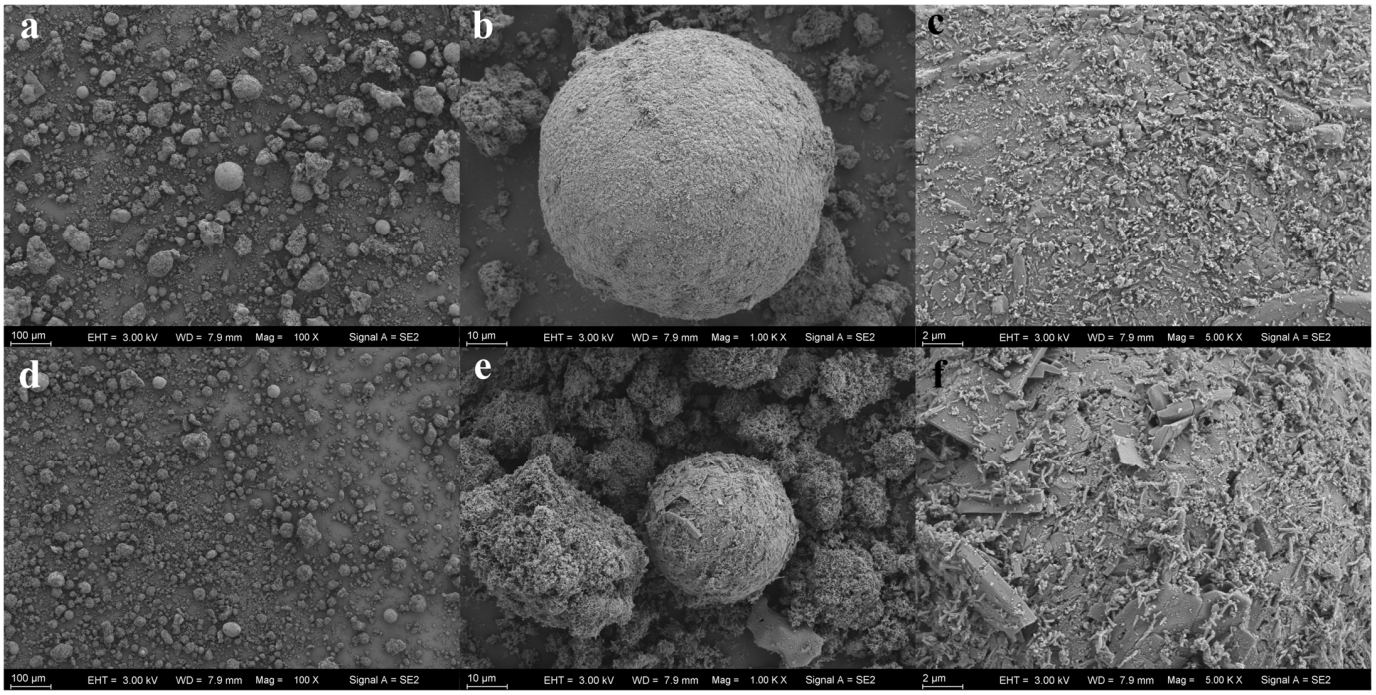

Figure 12. Comparison of SEM images of fly ash after primary leaching and after carbonate-assisted leaching. (**a**) After primary leaching (100 μm). (**b**) After primary leaching (10 μm). (**c**) After primary leaching (2 μm). (**d**) After carbonate-assisted leaching (100 μm). (**e**) After carbonate-assisted leaching (10 μm). (**f**) After carbonate-assisted leaching (2 μm).

This phenomenon is attributed to intense cavitation occurring during carbon dioxide passage, where drastic pressure changes impact the surfaces of fly ash, causing fragmentation. This process increases the contact area between fly ash particles and water, thereby enhancing both the leaching rate and efficiency.

3.5. Ultrasound-Assisted Leaching

The influence of ultrasonic waves on the leaching efficiency of chloride and calcium ions was determined to be negligible. Specifically, in the absence of ultrasonic intervention, the leaching rate of chloride ions was 86.89%, with a corresponding calcium ion concentration of 4101.5 mg/L. In contrast, applying 40 kHz ultrasonic waves resulted in a chloride ion leaching rate of 86.17% and a calcium ion concentration of 4101 mg/L. These findings indicate that ultrasonic treatment does not significantly enhance leaching efficiency under the conditions analyzed [10,43].

As shown in Figure 13, SEM images demonstrate that ultrasound-assisted leaching produces numerous small pits on fly ash particle surfaces compared to conventional primary leaching. Most needle-like and block-like protrusions fused into larger structures, with sizes reaching up to 15 μm in diameter and heights up to approximately 10 μm.

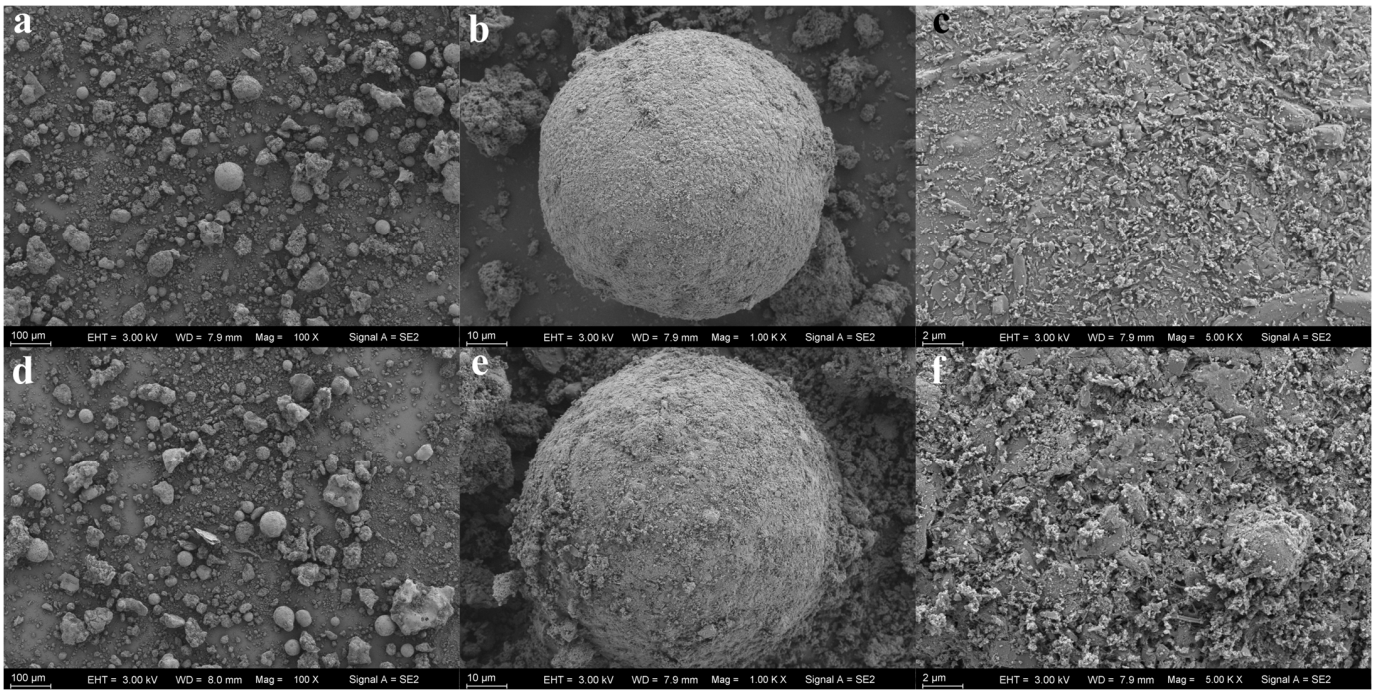

Figure 13. SEM images comparing fly ash after primary leaching and ultrasound-assisted leaching: (**a**) primary leaching (100 μm); (**b**) primary leaching (10 μm); (**c**) primary leaching (2 μm); (**d**) ultrasound-assisted leaching (100 μm); (**e**) ultrasound-assisted leaching (10 μm); (**f**) ultrasound-assisted leaching (2 μm).

This phenomenon increased the contact area between water and fly ash particle surfaces; however, inward-facing pits with small openings prevented effective contact with their inner walls due to surface tension [44,45]. Consequently, ultrasound-assisted leaching did not yield the expected results.

3.6. Particle Size Distribution

The particle size distribution data indicate an overall range from 0 to 10,000 μm, with the majority of diameters falling between 0 and 800 μm. Integral image analysis reveals that the full distribution is achieved at 724.44 μm for original fly ash, 478.63 μm for primary leached fly ash, and 120.23 μm for secondary leached fly ash. This demonstrates that leaching significantly affects fly ash particles, with secondary leaching having a more pronounced impact. Furthermore, log–log image curves indicate that most original and primary leached fly ash particles (>4%) are within the 40–90 μm range, while secondary leached fly ash particles predominantly range from 3 to 6 μm [33]. The primary leached fly ash curve reflects a reduction of the original curve, showing an approximate decrease of 0.2% across all particle sizes. In contrast, secondary leached fly ash diameters differ significantly from those of original and primary leached samples, with over 50% of particles larger than 35 μm disappearing (Figure 14).

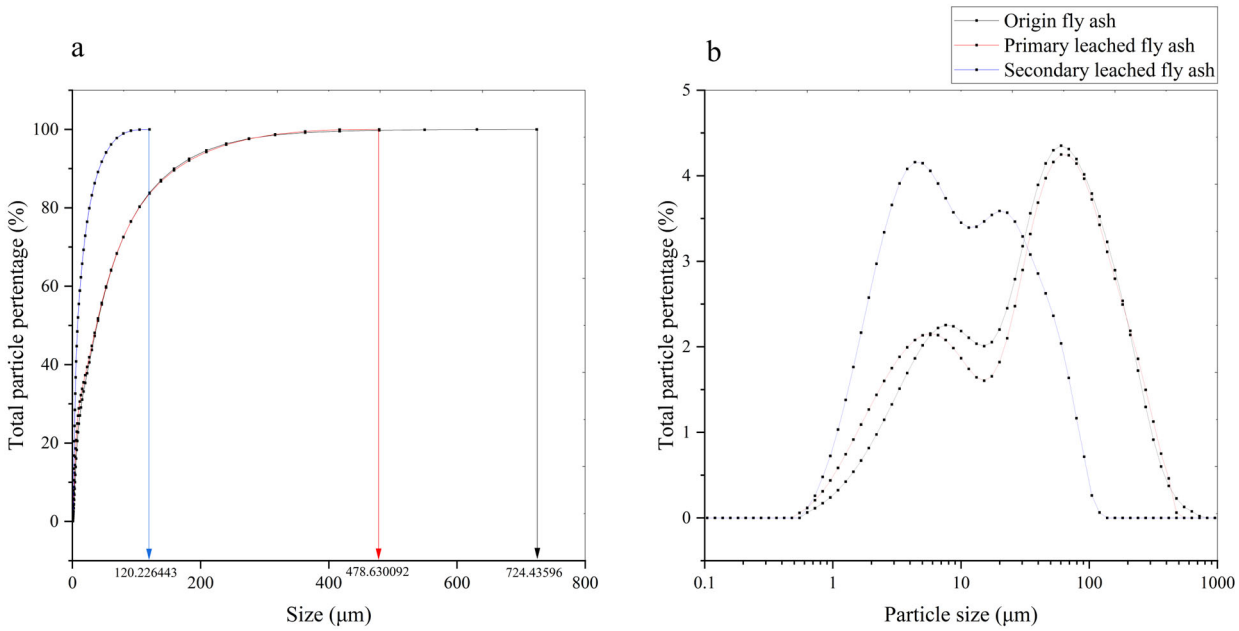

Figure 14. Particle size of the fly ash: (**a**) the integral of the available particle size range and the size at which 100% of the fly ash from the different batches is reached; (**b**) the logarithmic graph of the different batches of fly ash and the specific size distribution of the fly ash.

This suggests that soluble salts on the outer surfaces dissolved during water washing, reducing particle diameters; some particles composed entirely of soluble salts dissolved completely, leading to their disappearance. Because primary leaching does not achieve high efficiency, its curve resembles a reduced version of the original fly ash curve, but it is not significantly altered. Conversely, secondary leaching is sufficiently efficient to fully dissolve most soluble salts and disintegrate particles, resulting in substantial changes in particle diameter distribution [46].

4. Conclusions and Prospect

This study investigated various leaching methods to optimize the extraction of calcium and chloride from MSWI fly ash, with a particular focus on the role of salt in enhancing leaching efficiency. The key findings can be summarized as follows:

(1) Optimal leaching conditions were determined to be a 60 min leaching time, a 200 rpm stirring speed, a temperature of 30 °C, and a high liquid-to-solid (L/S) ratio.
(2) Secondary leaching improves ion extraction efficiency, whereas reverse secondary leaching (RSL) is less efficient but conserves water.
(3) A 6% NaCl solution concentration maximizes ion leaching; concentrations higher or lower than this threshold reduce calcium ion extraction.
(4) The addition of carbon dioxide enhances chloride ion leaching but reduces calcium ion extraction. The flow rate influences only the pH reduction and calcium hydroxide precipitation rates.
(5) Ultrasonic intervention has minimal impact on efficiency and can be considered negligible.

The various approaches explored in this study to optimize leaching efficiency, including RSL and the salt effect, consider both cost and environmental benefits in industrial production, thus conserving water resources while reducing time and economic costs. The leachate produced can be reused in industrial processes, such as flue gas carbon capture and electrolysis to produce high-purity calcium carbonate. In the carbon capture process, solids, toxic gases, and greenhouse gases like CH_4 and CO_2 are removed from industrial emissions. Leachate can serve as a solvent to absorb CO_2, reducing reliance on traditional

materials like amines and water and thus lowering costs and increasing treatment efficiency. During electrolysis, additional ions are incorporated to enhance efficiency in producing NaOH, Cl_2, and H_2.

Future research directions include exploring other catalysts, variations in pH levels, different ultrasound frequencies, and alternative solvent types, among other factors. Additionally, various characterization methods will be employed to examine relationships, such as that between particle size distribution and leaching efficiency. Understanding how different particle sizes influence dissolution rates and surface area exposure could lead to more effective processing methods.

Author Contributions: K.Z.: methodology, validation, writing—original draft. Y.X.: methodology, validation, formal analysis, writing—original draft and review. D.L.: writing—review and editing, supervision. J.Z.: writing—review and editing, supervision. M.S.: writing—review and editing, formal analysis. Y.T.: validation, formal analysis. All authors have read and agreed to the published version of the manuscript.

Funding: This research received no external funding.

Data Availability Statement: All the data had been stored in the ScienceDB database with the DOI https://doi.org/10.57760/sciencedb.13171.

Acknowledgments: We thank the Jiaxing Tongji Environmental Research Institution for providing the experimental site and equipment, and Jianfu Zhao, Guodong Yao, Guodong Ying, and Zhaojun Tang for their help with the experimental assist and manuscript review. We thank David Armstrong from the University of Toronto Mississauga for his input regarding the experimental design and data analysis. We thank Zhirui Chu from Queen's University and Zheng Cao, Haoyuan Yang, and Jodh Jassal from the University of Toronto Mississauga for their contributions to data collection, analysis, and statistical support. We thank Ying Su for her work in drawing and revising the images.

Conflicts of Interest: The authors declare that they have no known conflicts of interest.

References

1. Xiao, Y.; Huang, Y.; Cheng, H.; Zhu, Z.; Yu, M.; Xu, W.; Li, Z.; Zuo, W.; Zhou, H.; Jin, B. Advances and Outlook of Heavy Metal Treatment Technology from Municipal Solid Waste Incineration Fly Ash: A Review. *Energy Fuels* **2024**, *38*, 895–918. [CrossRef]
2. Chen, H.; Niu, F.; Wang, N. Research progress of dioxins and heavy metal pollution control technology in MSWI. *Clean Coal Technol.* **2021**, *27*, 59–75. [CrossRef]
3. Yadav, V.K.; Amari, A.; Wanale, S.G.; Osman, H.; Fulekar, M.H. Synthesis of Floral-Shaped Nanosilica from Coal Fly Ash and Its Application for the Remediation of Heavy Metals from Fly Ash Aqueous Solutions. *Sustainability* **2023**, *15*, 2612. [CrossRef]
4. Gadore, V.; Ahmaruzzaman, M. Fly ash–based nanocomposites: A potential material for effective photocatalytic degradation/elimination of emerging organic pollutants from aqueous stream. *Environ. Sci. Pollut. Res.* **2021**, *28*, 46910–46933. [CrossRef] [PubMed]
5. Thennarasan Latha, A.; Murugesan, B. Compressed stabilised earth block synergistically valorising municipal solid waste incinerator bottom ash and sisal fiber: Strength, durability and life cycle analysis. *Constr. Build. Mater.* **2024**, *441*, 137514. [CrossRef]
6. Thennarasan Latha, A.; Murugesan, B.; Kabeer, K.I.S.A. Valorisation of municipal solid waste incinerator bottom ash for the production of compressed stabilised earth blocks. *Constr. Build. Mater.* **2024**, *423*, 135827. [CrossRef]
7. Tkachenko, N.; Tang, K.; McCarten, M.; Reece, S.; Kampmann, D.; Hickey, C.; Bayaraa, M.; Foster, P.; Layman, C.; Rossi, C.; et al. Global database of cement production assets and upstream suppliers. *Sci. Data* **2023**, *10*, 696. [CrossRef] [PubMed]
8. Antonioni, G.; Dal Pozzo, A.; Guglielmi, D.; Tugnoli, A.; Cozzani, V. Enhanced modelling of heterogeneous gas–solid reactions in acid gas removal dry processes. *Chem. Eng. Sci.* **2016**, *148*, 140–154. [CrossRef]
9. Cho, B.H.; Nam, B.H.; An, J.; Youn, H. Municipal Solid Waste Incineration (MSWI) Ashes as Construction Materials—A Review. *Materials* **2020**, *13*, 3143. [CrossRef] [PubMed]
10. Zha, F.; Dai, J.; Wang, S.; Jin, S.; Liu, Z.; Wang, X.; Zhang, S.; Hu, Y.; Xu, G.; Yang, L. Effect on Leaching Characteristics of Fly Ash Treated by an Ultrasound-assisted Water-washing or Hydrochloric Acid-extraction. *Environ. Sci. Technol.* **2022**, *45*, 223–231. [CrossRef]

11. Xu, P.; Zhao, Q.; Qiu, W.; Xue, Y.; Li, N. Microstructure and Strength of Alkali-Activated Bricks Containing Municipal Solid Waste Incineration (MSWI) Fly Ash Developed as Construction Materials. *Sustainability* **2018**, *11*, 1283. [CrossRef]
12. Ma, B.; Yang, H.; Sun, Z.; Wang, Y. Research progress on separation and extraction technologies of chlorine salts and heavy metals from municipal solid waste incineration fly ash. *Environ. Chem.* **2024**, 790–805. [CrossRef]
13. Marieta, C.; Guerrero, A.; Leon, I. Municipal solid waste incineration fly ash to produce eco-friendly binders for sustainable building construction. *Waste Manag.* **2021**, *120*, 114–124. [CrossRef] [PubMed]
14. Chang, W.; Liu, H.; Jiang, X. Study on dechlorination and heavy metal leaching characteristics of MSWI fly ash during water-washing. *Inorg. Chem. Ind.* **2022**, *54*, 113–118. [CrossRef]
15. Clavier, K.A.; Paris, J.M.; Ferraro, C.C.; Townsend, T.G. Opportunities and challenges associated with using municipal waste incineration ash as a raw ingredient in cement production—A review. *Resour. Conserv. Recycl.* **2020**, *160*, 104888. [CrossRef]
16. He, Y.; Zhang, J.; Yue, Y.; Qian, G. Research progress on treatment technology and resource utilization of waste solution used in fly ash washing. *Environ. Prot. Sci.* **2023**, 1–9. [CrossRef]
17. Assi, A.; Federici, S.; Bilo, F.; Zacco, A.; Depero, L.E.; Bontempi, E. Increased Sustainability of Carbon Dioxide Mineral Sequestration by a Technology Involving Fly Ash Stabilization. *Materials* **2019**, *12*, 2714. [CrossRef]
18. Xu, T.; Wang, L.a.; Zeng, Y.; Zhao, X.; Wang, L.; Zhan, X.; Li, T.; Yang, L. Characterization of typical heavy metals in pyrolysis MSWI fly ash. *Environ. Technol.* **2019**, *40*, 3502–3511. [CrossRef] [PubMed]
19. Huang, J.; Jin, Y. Fate of Cl and chlorination mechanism during municipal solid waste incineration fly ash reutilization using thermal treatment: A review. *Environ. Sci. Pollut. Res.* **2024**, *31*, 3320–3342. [CrossRef]
20. Liang, D.; Wang, F.; Lv, G. The Resource Utilization and Environmental Assessment of MSWI Fly Ash with Solidification and Stabilization: A Review. *Waste Biomass Valorization* **2024**, *15*, 37–56. [CrossRef]
21. Hatzilyberis, K.; Tsakanika, L.-A.; Lymperopoulou, T.; Georgiou, P.; Kiskira, K.; Tsopelas, F.; Ochsenkühn, K.-M.; Ochsenkühn-Petropoulou, M. Design of an advanced hydrometallurgy process for the intensified and optimized industrial recovery of scandium from bauxite residue. *Chem. Eng. Process.-Process Intensif.* **2020**, *155*, 108015. [CrossRef]
22. Falaciński, P.; Wojtkowska, M. The use of extraction methods to assess the immobilization of metals in hardening slurries. *Arch. Environ. Prot.* **2021**, *47*, 60–70. [CrossRef]
23. Lin, T.-H.; Siao, H.-J.; Gau, S.-H.; Kuo, J.-H.; Li, M.-G.; Sun, C.-J. Life-Cycle Assessment of Municipal Solid Waste Incineration Fly Ash Recycling as a Feedstock for Brick Manufacturing. *Sustainability* **2023**, *15*, 10284. [CrossRef]
24. Han, S.-J.; Yoo, M.; Kim, D.-W.; Wee, J.-H. Carbon Dioxide Capture Using Calcium Hydroxide Aqueous Solution as the Absorbent. *Energy Fuels* **2011**, *25*, 3825–3834. [CrossRef]
25. Weibel, G.; Eggenberger, U.; Kulik, D.A.; Hummel, W.; Schlumberger, S.; Klink, W.; Fisch, M.; Mäder, U.K. Extraction of heavy metals from MSWI fly ash using hydrochloric acid and sodium chloride solution. *Waste Manag.* **2018**, *76*, 457–471. [CrossRef]
26. Ebert, B.A.R.; Kirkelund, G.M. Effects of Chlorides and Sulphates on Heavy Metal Leaching from Mortar with Raw and Electrodialytically Treated MSWI Fly Ash. *Waste Biomass Valorization* **2022**, *13*, 2673–2688. [CrossRef] [PubMed]
27. *GB 11896-89*; Water Quality-Determination of Chloride- Silver Nitrate Titration Method. Standardization Administration of the People's Republic of China: Beijing, China, 1990.
28. *GB/T 15452-2009*; Industrial Circulating Cooling Water—Determination of Calcium and Magnesium—EDTA Titration Method. Standardization Administration of the People's Republic of China: Beijing, China, 2009.
29. *DZ/T 0064.49-93*; Test Method of Groundwater Quality. Ministry of Geology and Mineral Resources of the People's Republic of China: Beijing, China, 1993.
30. Jiménez, A.; Rives, V.; Vicente, M.A. Thermal study of the hydrocalumite–katoite–calcite system. *Thermochim. Acta* **2022**, *713*, 179242. [CrossRef]
31. Nakamura, T.; Shibata, E. Establishment of Physicochemical Database of Oxyhalogen Compounds for Advanced Recycling. 2007–2009. Available online: https://kaken.nii.ac.jp/en/grant/KAKENHI-PROJECT-19206097 (accessed on 11 March 2024).
32. Georgakopoulos, E.; Santos, R.M.; Chiang, Y.W.; Manovic, V. Two-way Valorization of Blast Furnace Slag: Synthesis of Precipitated Calcium Carbonate and Zeolitic Heavy Metal Adsorbent. *J. Vis. Exp.* **2017**, e55062. [CrossRef]
33. Huang, H.; Liu, W.; Zhang, L.; Fang, J.; Xu, F.; Bu, S.; Xu, W.; Xu, C.; Yao, H.; Ma, Z. A microscopic and quantitative analysis on the separation of chloride ion by fly ash washing: Effect of liquid-to-solid ratio, washing time and temperature. *Environ. Sci. Pollut. Res.* **2022**, *29*, 36208–36215. [CrossRef] [PubMed]
34. Li, B.; Gao, L.; Ru, C.; Han, Z.; Liu, Y. Simulation of MSWI Fly Ash Washing Process and Calculation of Washing Loss Rate. *Environ. Sanit. Eng.* **2023**, *31*, 80–84. [CrossRef]
35. Liu, W.; Xu, H.; Shi, X.; Yang, X.; Chen, Y.; Cheng, J.F.; Li, G. Equilibrium concentration of calcium hydroxide in CaCl 2-Ca(OH) 2-H 2O system. *Zhongguo Youse Jinshu Xuebao/Chin. J. Nonferrous Met.* **2012**, *22*, 2656–2661.
36. Yan, M.; Jiang, J.; Zheng, R.; Yu, C.; Zhou, Z.; Hantoko, D. Experimental study on the washing characteristics of fly ash from municipal solid waste incineration. *Waste Manag. Res.* **2021**, *40*, 1212–1219. [CrossRef]

37. Yang, X.; Feng, Y.; Rong, H.; Liang, J.; Zhang, G.; Huang, Y. The leaching-deterioration properties and leaching mechanism of cement mortar under dry-wet cycles. *Constr. Build. Mater.* **2023**, *400*, 132672. [CrossRef]
38. Chen, W.; Wang, Y.; Sun, Y.; Fang, G.; Li, Y. Release of soluble ions and heavy metal during fly ash washing by deionized water and sodium carbonate solution. *Chemosphere* **2022**, *307*, 135860. [CrossRef] [PubMed]
39. Liu, Z.; Yang, Y.; Zhang, Y.; Yue, Y.; Zhang, J.; Qian, G. Controlling Role of CaClOH in the Process of Dechlorination for Municipal Solid Incineration Fly Ash Utilization. *ACS EST Eng.* **2022**, *2*, 2150–2158. [CrossRef]
40. Lamprakou, Z.; Bi, H.; Weinell, C.E.; Dam-Johansen, K. Encapsulated Corrosion Inhibitive Pigment for Smart Epoxy Coating Development: An Investigation of Leaching Behavior of Inhibitive Ions. *ACS Omega* **2023**, *8*, 14420–14429. [CrossRef] [PubMed]
41. Wei, Y.-m.; Yao, R.-x.; Chen, S.; Zhou, H.-l.; Liu, S.-j. Removal of chloride from MSWI fly ash: A comparison of accelerated carbonation and water flushing. *Environ. Chem.* **2021**, *41*, 4184–4192.
42. Lun, D.; Yuan, T.; Yang, X.; Rong, H.; Shi, J.; Pan, M. Effect of Fly Ash on Leaching Characteristics of Cement-Stabilized Macadam Base. *Materials* **2021**, *14*, 5935. [CrossRef] [PubMed]
43. Lim, J.-L.; Kim, S.-W.; Shin, H.-S.; Okuda, T.; Okada, M. Leaching Behavior of Lead from Ultrasonically Treated MSWI Fly Ash. *J. Environ. Sci. Health Part A* **2004**, *39*, 1587–1599. [CrossRef]
44. Al-Sibai, M.; Adey, M.A.; Rose, D.A. Movement of solute through a porous medium under intermittent leaching. *Eur. J. Soil Sci.* **1997**, *48*, 711–725. [CrossRef]
45. Yu, S.; Wu, A.; Wang, Y. Insight into the structural evolution of porous and fractured media by forced aeration during heap leaching. *Int. J. Min. Sci. Technol.* **2019**, *29*, 803–807. [CrossRef]
46. Zhang, Z.; Cai, W.; Hu, Y.; Yang, K.; Zheng, Y.; Fang, C.; Ma, C.; Tan, Y. Ecological Risk Assessment and Influencing Factors of Heavy-Metal Leaching From Coal-Based Solid Waste Fly Ash. *Front. Chem.* **2022**, *10*, 932133. [CrossRef] [PubMed]